Optical Materials 148 (2024) 114950

Contents lists available at ScienceDirect

Optical Materials

journal homepage: www.elsevier.com/locate/optmat

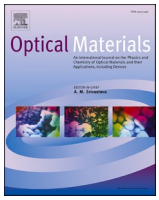

Review article

Spectroscopic characteristics and gain cross-section profiles of erbium-doped boro-tellurite glasses for optical amplifier applications

B. Kiran Kumar [a,b], P. Reddi Babu [a], Esra Kavaz [c], Yuwaraj K. Kshetri [d], Tae-Ho Kim [d], Virgilio de Carvalho dos Anjos [e], B. Deva Prasad Raju [a,*]

[a] Department of Physics, Sri Venkateswara University, Tirupati, 517 502, India
[b] Department of Physics, Government Degree College, Rayachoty, 516 269, India
[c] Department of Physics, Ataturk University, Erzurum, 25240, Turkey
[d] Research Center for Green Advance Materials, Sun Moon University, Chungnam, 31460, Republic of Korea
[e] Departamento de Física – ICE, Universidade Federal de Juiz de Fora, Campus Universitário, SN, Juiz de Fora, MG, 36036-330, Brazil

ARTICLE INFO

Keywords:
Boro-tellurite glasses
Er^{3+} ions
Radiative characteristics
1.53 μm lasers
Gain-cross-section
Optical amplifiers

ABSTRACT

A series of glass compositions (60-x) B_2O_3–$10TeO_2$–$15BaCO_3$–$15MgF_2$–xEr_2O_3 with diverse quantities of erbium ions (Er^{3+}) was synthesized using the melt quenching method and the samples were subjected to thorough characterization to explore their optical and structural properties. In order to ascertain the amorphous nature of the glass and acquire a deeper understanding of its chemical bonding, conventional methods of characterization, such as X-ray diffraction and Fourier transform infrared spectroscopy, were utilized. The Judd-Ofelt intensity parameters were computed using the absorption spectra of glasses doped with Er^{3+}, providing vital information about the local environment and coordination of Er^{3+} ions in the glass matrix. The glasses underwent the collection of near -infrared (NIR) emission spectra. Following this, an analysis was carried out to look into and understand the spectral properties, emission cross-section, and gain coefficient parameters of the glasses. The spectra obtained discernible characteristics, notably a significant near-infrared (NIR) band associated with the transition between the $^4I_{13/2}$ and $^4I_{15/2}$ states. This band was seen to have a central wavelength of 1530 nm. This emission band spanned the wavelengths commonly used in optical communication systems (S + C) -bands, making these glasses suitable candidates for applications such as wavelength division multiplexing (WDM). These results suggest that the boro-tellurite glass may have potential use in photonic devices designed for near-infrared applications, including optical communication systems.

1. Introduction

Recent breakthroughs have increased demand for glasses doped with rare earth (RE) elements for variety of photonic applications, laser technology, medical diagnosis, solar cells and optical communications. The heightened focus can be attributed mostly to the attractive luminous characteristics that have been observed in these materials notable throughout the visible and near-infrared (NIR) spectra [1]. The research has concentrated on identifying host matrices that possess key properties such as mechanical durability, chemical stability, thermal diffusivity, thermal conductivity and low phonon energy. Finding suitable host materials that operate effectively in the infrared (IR) region is crucial to enhance luminescence efficiency.

Borate glasses have gained recognition as a viable choice for photonic applications due to their distinctive characteristics, which encompasses a lower melting point, remarkable solubility of rare earth ions, favorable optical transparency, improved thermal stability and cost-effectiveness. The fundamental building blocks of borate glass networks consist of triangular [BO_3] and tetrahedral [BO_4] units. Significant alterations in the bonding interactions between oxygen and anions, specifically the metal-oxygen (M−O) bonds, as well as the transition from bridging to non-bridging oxygen (NBO) connections, have been discovered to have a notable impact on both structural configuration and optical characteristics of glass systems [2–5]. Furthermore, the comparatively elevated phonon energy exhibited by borate glass has the potential to detrimentally impact both the efficiency of luminescence and the lifetimes of fluorescence. To mitigate these effects, TeO_2 is often introduced to increase the refractive index, reduce

* Corresponding author.
E-mail address: drdevaprasadraju@gmail.com (B. Deva Prasad Raju).

https://doi.org/10.1016/j.optmat.2024.114950
Received 2 December 2023; Received in revised form 16 January 2024; Accepted 18 January 2024

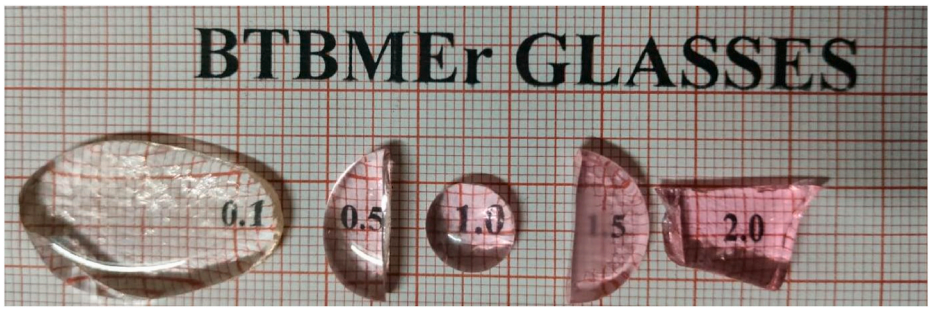

Fig. 1. The photograph of different concentration of Er-doped borotellurite glasses.

Table 1
Physical features of BTBMEr glasses.

Physical properties	BTBMEr01	BTBMEr05	BTBMEr10	BTBMEr15	BTBMEr20
Density (g/cm^3)	3.0476	3.2095	3.2123	3.2412	3.313
Thickness (cm)	0.3891	0.4624	0.3896	0.3818	0.3766
Refractive index (n)	1.653	1.654	1.655	1.656	1.657
Dielectric constant (ϵ)	2.7324	2.7357	2.7390	2.7423	2.7456
Concentration N (mol/lit)	0.0241	0.1200	0.2438	0.3760	0.5009
Concentration N (ions/c.c × 10^{20})	0.29050	1.4456	2.9363	4.5297	6.6034
Reflection loss (%)	354.1338	357.2756	360.4495	363.656	366.8956
Molar volume V_m (cm^3/mol)	42.4469	40.6283	40.9958	41.0296	40.5311
Polaran Radius R_p (A^0)	13.1115	7.6798	6.0642	5.2482	4.6285
Inter Ionic distance R_i (A^0)	32.5300	19.0539	15.0453	13.0210	11.4836
Field strength F (×10^{-14} cm^{-2})	1.7451	5.0865	8.1580	10.8918	14.0033
Molar Refractivity (cm^{-3})	15.5386	14.8909	15.0438	15.0743	14.9090
Electronic Polarizability (× 10^{-24} cm^3)	6.16	5.90	5.96	5.97	5.91

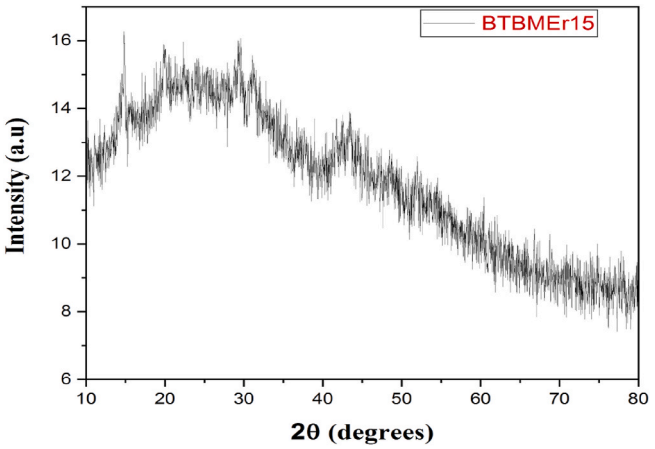

Fig. 2. XRD Spectrum of BTBMEr15glass sample.

hygroscopicity, and lower phonon energy [3–10]. Boro-tellurite glasses, therefore, exhibit desirable thermal and optical characteristics. The addition of alkaline oxides like $BaCO_3$ to borate glasses can further modify the glass network, reducing phonon energy and enhancing structural stability [11,12]. The use of MgF_4, which yields glass networks including MgF_4 tetrahedral units, has been found to augment the solubility of rare earth ions inside the glass matrix, while simultaneously reducing its viscosity. The use of fluorides into glass matrices has been widely recognized for its ability to enhance emission characteristics [13,14]. Hence, in this study, we have chosen to work with a composition comprising B_2O_3, TeO_2, $BaCO_3$ and MgF_2.

Among the RE elements, erbium stands out for its unique 1.53 μm emission within the NIR spectrum, long luminescence lifetime, narrow emission bandwidth and large absorption cross-section [15–17]. Despite the existence of prior studies on erbium-doped glasses, additional research must be carried out aimed at enhancing the structural, thermal and spectroscopic features of erbium-doped boro-tellurite glasses through compositional alterations. The present study involves the development of a novel series of erbium-doped boro-tellurite glasses, aiming to investigate their spectroscopic and luminescent properties. Thorough research and assessment have been carried out on crucial parameters, including Judd-Ofelt parameters, absorption cross-section, stimulated emission cross-section, gain bandwidth and lifetime.

2. Experimental techniques

2.1. Sample preparations

In this study, diverse quantities of Er^{3+} ions were introduced into boro-tellurite glass matrices through the utilization of high quality (99.9 %) chemical precursors. These precursors include barium carbonate ($BaCO_3$), magnesium fluoride (MgF_2), boron trioxide (B_2O_3), tellurium dioxide (TeO_2) and erbium trioxide (Er_2O_3). The host glass composition is represented by (60-x) B_2O_3– 10 TeO_2– 15$BaCO_3$– 15 MgF_2–x Er_2O_3, where x represents a variable concentration of Er^{3+} ions. A traditional melting and rapid cooling method was employed to fabricate the glasses; after which they were labeled accordingly for identification as follows;

A) 59.9B_2O_3– 10TeO_2– 15$BaCO_3$– 15MgF_2– 0.1 Er_2O_3:BTBMEr01
B) 59.5B_2O_3– 10 TeO_2– 15$BaCO_3$– 15MgF_2– 0.5 Er_2O_3: BTBMEr05
C) 59B_2O_3– 10 TeO_2– 15$BaCO_3$– 15MgF_2– 1Er_2O_3: BTBMEr10
D) 58.5B_2O_3– 10 TeO_2– 15$BaCO_3$– 15MgF_2– 1.5 Er_2O_3: BTBMEr15
E) 58B_2O_3– 10 TeO_2– 15$BaCO_3$– 15MgF_2– 2 Er_2O_3: BTBMEr20

According to the above compositions, each constituent compound was carefully measured to a batch composition of 20 g. Subsequently, these compounds were finely pulverized using an agate mortar to produce homogeneous powder. It was then undergoing a 90 min heating process at a temperature of 1200 °C, utilizing an alumina crucible positioned within a furnace chamber to obtain molten melt from the uniform powder. To reduce the occurrence of air bubbles and alleviate

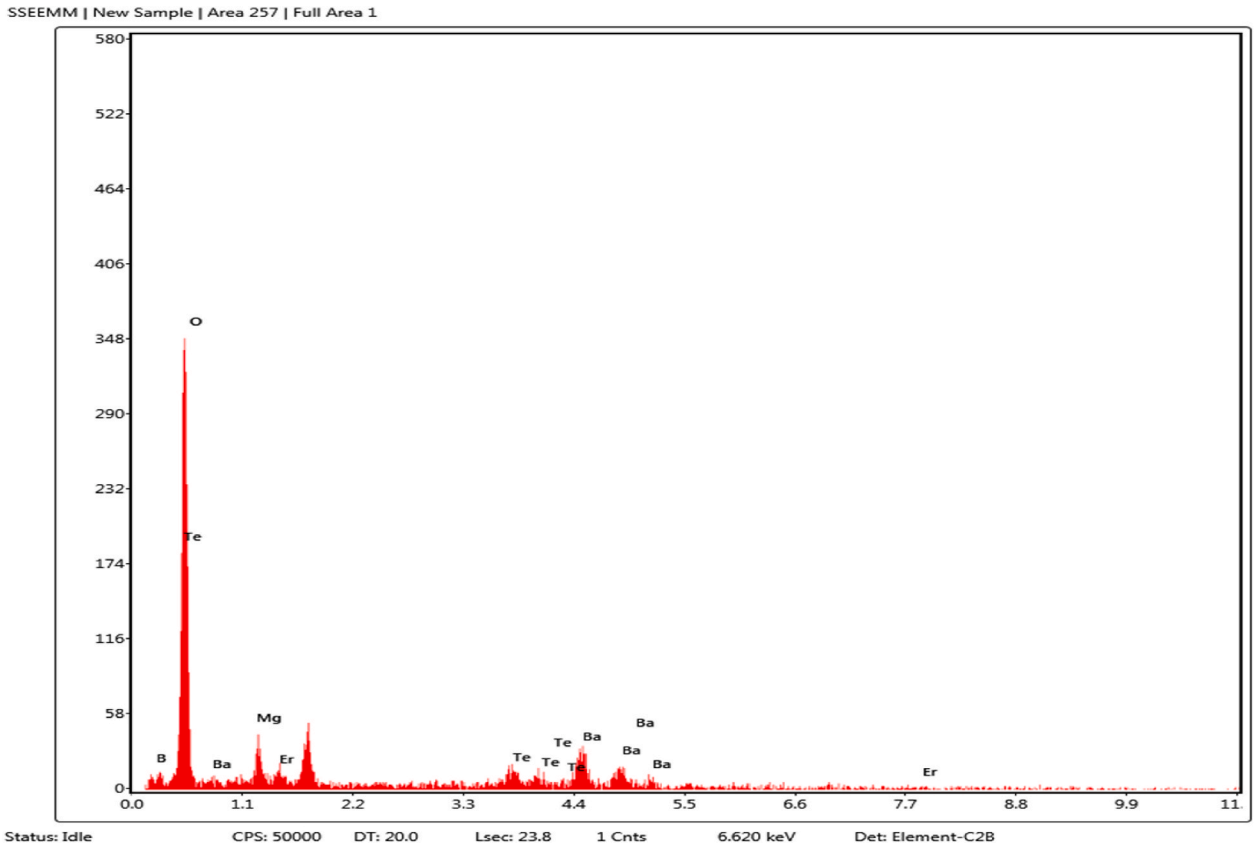

Fig. 3. EDX spectrum of the BTBMEr15 glass.

Table 2
EDX measurements of element weights in BTBMEr15 glass.

Element	Weight %	Atomic %
B K	6.04	17.66
O K	32.02	63.30
Mg K	4.74	6.16
TeL	12.62	3.13
BaL	32.14	7.40
ErL.	12.45	2.35
Total	100	100

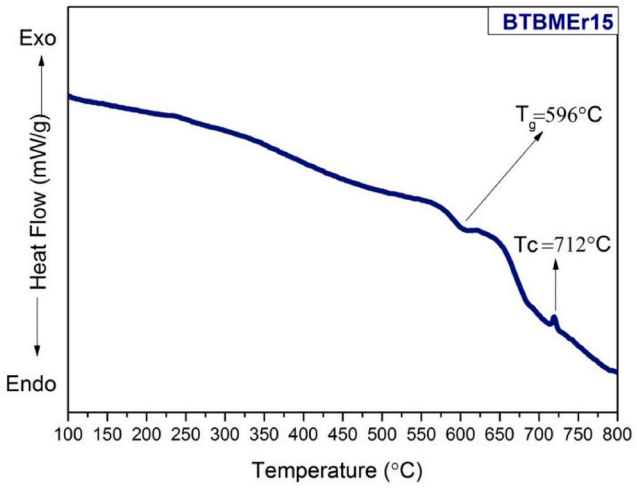

Fig. 4. DSC pattern of BTBMEr15 glass sample.

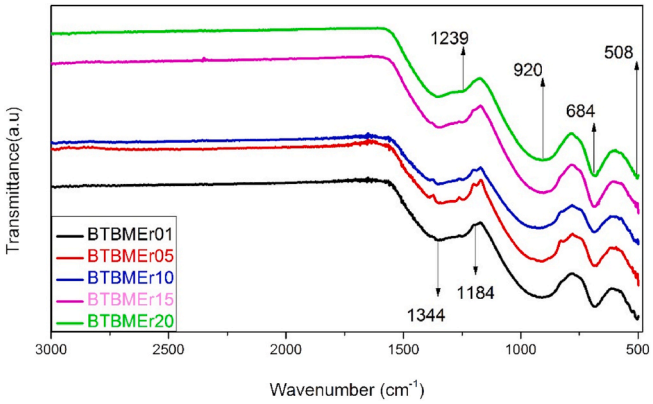

Fig. 5. FTIR spectra of BTBMEr glasses.

mechanical stress, the liquid material was meticulously poured onto a sturdy brass plate that has been preheated. Following this, an extended annealing process at 450 °C was carried out, with the samples being annealed for a duration of 7 h. Subsequently, the prepared glass samples underwent cooling process, gradually reaching room temperature. The glass samples were subjected to a polishing procedure in order to achieve uniform thickness. These samples were then utilized for various optical characterization techniques. Fig. 1 presents visual representations of the aforementioned samples.

2.2. Characterizations

Archimedes method was employed to assess the density of the glass samples, with xylene serving as the immersion liquid [18,19]. Abbe's

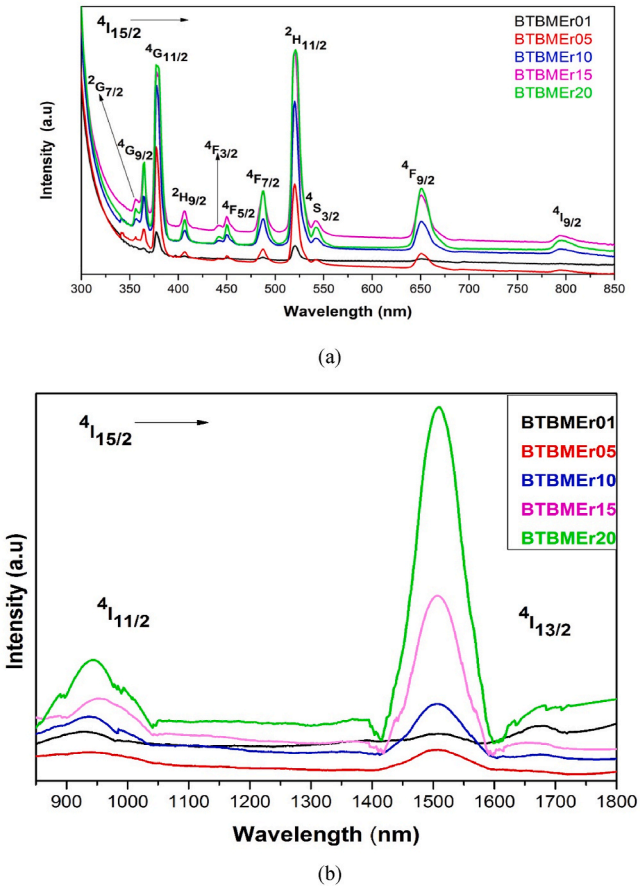

Fig. 6. (a) UV–Visible, (b)NIR absorption spectra of BTBMEr glasses.

refractometer, operating at a sodium wavelength of 589 nm, was utilized to ascertain the refractive index. This process involved employing mono bromonaphtalene as the contact liquid. RIGAKU X-ray diffractometer was utilized to acquire X-ray diffraction (XRD) spectrum, spanning a 2θ range of 10°-80°.The EDAX analysis was conducted using the Oxford INCA FETX3 instrument. BRUKER ALPHA-II FTIR spectrometer, characterized by a 2 cm^{-1} resolution, was employed for the acquisition of FTIR spectra. The measurement encompassed the frequency range from 500 to 3000 cm^{-1}. The UV-VIS-NIR Spectrometer, namely the JASCO model V-570, was utilized to acquire the optical absorption spectra. The FLS-980 Fluorog-3 spectrometer was utilized for the collection of photoluminescence spectra.

3. Results and discussions

3.1. Physical properties

The glass samples, which were prepared, underwent a comprehensive evaluation. Key physical characteristic, including average molecular weight, density, refractive index (n), dielectric constant (ϵ), RE concentration (N), molar volume (V_m), polaron radius (R_p), reflection loss, inter ionic distance (R_i), molar refractivity, field strength (F) and electronic polarizability were assessed by using established formulae from the literature [20–22]. These findings have been compiled and presented in Table 1. The observed density trend in this investigation can be ascribed to the escalating concentration of Er_2O_3, resulting in a corresponding augmentation in the quantity of Er^{3+} ions within a certain volume unit. Consistent with previous studies in the literature [23,24]. It was observed that the refractive index exhibited an upward trend as the concentration of Er^{3+} ions increased.

3.2. Structural analysis

The XRD pattern depicted in Fig. 2 illustrates the absence of distinct peaks in the BTBMEr15 glass. The lack of distinct peaks observed indicates that the sample under investigation possesses a non-crystalline structure [25–27]. Fig. 3 presents an energy dispersive X-ray (EDX) spectrum for the BTBMEr15 glass, accompanied by a tabular representation of the weight percentages of the component composition in Table 2. This observation provides evidence for the existence of the individual components inside the composition of the glass. Fig. 4 illustrates the Differential Scanning Calorimetry (DSC) curve of the BBMEr15 sample. The chart clearly illustrates that the glass transition temperature (T_g) is observed at a value of 596 °C. Whilst the crystallization temperature (T_c) is observed at a value of 712 °C. The thermal stability of glass is typically defined as the difference between T_c and T_g [28];

$$\Delta T = T_c - T_g \quad (1)$$

Generally, the greater the value of ΔT, the more stable the glass. In the case of BTBMEr15, the ΔT is 116 °C, at which BTBMEr15 is classified as stable glass [29]. These results confirm preparations of the samples yielded thermally stable and rigid glass [30,31].

In Fig. 5, the FTIR spectra of BTBMEr glasses were showcased. The spectral analysis encompassed a wavenumber spectrum of 500–3000 cm^{-1} with the objective of identifying the several distinct functional

Table 3
Experimental (f_{exp}) and calculated (f_{cal}) spectral intensities of erbium ions of various absorption bands in the BTBMEr glass samples.

S. No	Absorption transition	Band positions		Oscillator strengths (x10^{-6})									
				BTBMEr01		BTBMEr05		BTBMEr10		BTBMEr15		BTBMEr20	
		Wavelength (nm)	Wavenumber (cm^{-1})	f_{exp}	f_{cal}	f_{exp}	f_{cal}	f_{exp}	f_{cal}	f_{exp}	f_{cal}	f_{exp}	f_{cal}
1	$^4I_{15/2} \rightarrow {}^2G_{7/2}$	356	28090	–	–	0.4457	0.3866	0.4525	0.3645	0.4716	0.6687	1.4994	1.1163
2	$^4I_{15/2} \rightarrow {}^4G_{9/2}$	364	27472	0.7145	0.6268	0.5693	0.2082	0.7378	0.3002	1.0482	0.8272	1.3579	0.0544
3	$^4I_{15/2} \rightarrow {}^4G_{11/2}$	378	26455	10.5420	9.4862	5.2011	5.0001	6.7532	5.0564	5.1601	4.0556	4.7375	4.1865
4	$^4I_{15/2} \rightarrow {}^2H_{9/2}$	406	24630	0.6155	0.2831	0.6687	0.6692	0.8010	0.6012	1.2398	1.1659	1.9712	1.2463
5	$^4I_{15/2} \rightarrow {}^4F_{3/2}$	441	22676	–	–	0.1137	0.3550	0.4230	0.1167	0.6240	0.1304	1.1048	0.7010
6	$^4I_{15/2} \rightarrow {}^4F_{5/2}$	450	22222	0.5012	0.0393	0.2829	0.1804	0.7854	0.2274	1.3063	1.0730	0.3008	0.6418
7	$^4I_{15/2} \rightarrow {}^4F_{7/2}$	488	20492	2.9793	1.0144	1.6072	0.4852	0.7935	0.7231	2.9069	1.5435	0.8179	1.1718
8	$^4I_{15/2} \rightarrow {}^2H_{11/2}$	521	19194	5.3542	4.3932	2.5515	2.3212	3.6292	3.34112	3.3672	2.6272	3.0804	2.6619
9	$^4I_{15/2} \rightarrow {}^4S_{3/2}$	542	18450	–	–	0.1208	0.0520	0.5752	0.2982	0.8809	0.8325	1.5148	1.2917
10	$^4I_{15/2} \rightarrow {}^4F_{9/2}$	651	15361	–	–	0.7181	0.6136	0.8331	0.7957	0.8952	0.8973	1.9383	1.6057
11	$^4I_{15/2} \rightarrow {}^4I_{9/2}$	795	12579	–	–	0.1116	0.0534	0.1860	0.0466	0.1447	0.1028	0.3449	0.1854
12	$^4I_{15/2} \rightarrow {}^4I_{11/2}$	968	10331	13.4888	12.524	1.7597	0.9799	1.5362	0.6894	1.4338	0.9487	2.2780	1.5918
13	$^4I_{15/2} \rightarrow {}^4I_{13/2}$	1508	6631	1.1126	0.8624	1.1323	1.1269	1.4602	1.3992	2.2825	2.0222	3.9879	3.4048
				$\delta_{rms} = \pm 0.307$		$\delta_{rms} = \pm 0.475$		$\delta_{rms} = \pm 0.472$		$\delta_{rms} = \pm 0.642$		$\delta_{rms} = \pm 0.330$	

Table 4
Comparison of J-O parameters (Ω_λ x 10^{-20} cm^2) in various Er_2O_3 doped glasses with BTBMEr glass samples.

Glass host	Ω_2	Ω_4	Ω_6	$\chi = \Omega_4/\Omega_6$	Trend	Ref
BTBMEr01	6.6658	2.0356	2.1201	0.9601	$\Omega_2 > \Omega_6 > \Omega_4$	Present Work
BTBMEr05	7.0369	2.1168	2.2018	0.9614	$\Omega_2 > \Omega_6 > \Omega_4$	Present Work
BTBMEr10	7.2802	2.1242	2.2420	0.9474	$\Omega_2 > \Omega_6 > \Omega_4$	Present Work
BTBMEr15	7.6046	2.1634	2.7880	0.7759	$\Omega_2 > \Omega_6 > \Omega_4$	Present Work
BTBMEr20	7.9266	2.5736	3.6218	0.7106	$\Omega_2 > \Omega_6 > \Omega$	Present Work
BTNME4	3.60	1.32	1.82	0.7252	$\Omega_2 > \Omega_6 > \Omega_4$	[16]
SBNCEr05	6.69	3.08	3.28	0.9390	$\Omega_2 > \Omega_6 > \Omega_4$	[20]
LBBPE05	8.734	2.243	2.700	0.8307	$\Omega_2 > \Omega_6 > \Omega_4$	[28]
ErAg0.8-15	10.38	3.49	3.53	0.9887	$\Omega_2 > \Omega_6 > \Omega_4$	[41]
TZNEr10	5.98	1.32	1.47	0.8979	$\Omega_2 > \Omega_6 > \Omega_4$	[42]
TZN	5.757	1.106	1.299	0.8514	$\Omega_2 > \Omega_6 > \Omega_4$	[44]
KTFPEr10	5.086	0.693	1.453	0.4769	$\Omega_2 > \Omega_6 > \Omega_4$	[45]
NaTFPEr10	5.918	1.070	1.441	0.7425	$\Omega_2 > \Omega_6 > \Omega_4$	[45]
LiTFPEr10	4.697	1.210	1.296	0.9336	$\Omega_2 > \Omega_6 > \Omega_4$	[45]
LBTAFEr10	5.89	1.10	1.47	0.7482	$\Omega_2 > \Omega_6 > \Omega_4$	[46]
ZMBEr10	5.56	1.44	2.15	0.6697	$\Omega_2 > \Omega_6 > \Omega_4$	[47]
PKAPbEr10	4.79	0.79	1.22	0.6475	$\Omega_2 > \Omega_6 > \Omega_4$	[48]
LBZEr05	4.31	0.26	2.13	0.1220	$\Omega_2 > \Omega_6 > \Omega_4$	[49]

groups present. The study identified six discrete positions that exhibited alignment with the band positions reported at 508, 684, 920, 1184, 1239 and 1344 cm^{-1}. The band recorded at a wavenumber of around 508 cm^{-1} is linked to the stretching vibrations that takes place within the TeO_3 pyramids [30,32]. The spectrum characteristic detected at a wavenumber of 684 cm^{-1} is attributed to the bending vibrations of the Te–O bond found in both TeO_3 and TeO_6 structural units, as well as the flexing vibrations of O_3B-O-BO_3 [32–35]. The origin of the spectral bands detected at 920 and 1184 cm^{-1} has been proposed to be attributed to the vibrational motion of Te–O–Te bonds, arising from the presence of non-equivalent Te–O bonds inside TeO_3 molecular units [27,35]. The structural peak observed at a wavenumber of 1239 cm^{-1} is associated with the stretching vibrations of B–O bonds in BO_3 units. These units are found in both meta and ortho borate groups. The peak detected at a wavenumber of 1344 cm^{-1} is attributed to the vibrational stretching of B–O bonds found in BO_3 units that are connected with metaborate, pyro borate, and orthoborate groups [21]. The recognition of a prominent peak at around 800 cm^{-1}, which often linked to boroxol rings, is universally accepted in pure borate. Nevertheless, this specific composition is devoid of said characteristic attribute. The lack of these structural elements within the glass is indicated by their absence.

3.3. Optical absorption analysis

The optical spectra observed in glasses doped with rare earth elements arise from two absorption mechanisms. Intrinsic absorption is one of the first mechanisms across the range of wavelengths. An extrinsic absorption mechanism occurs when the rare earth ions undergo intra-electronic transitions, particularly within their 4f electron shell [27]. At standard room temperature, and spanning a wavelength range from 300 to 1800 nm, Fig. 6 (a), (b) illustrates absorption spectra of the UV–visible and NIR regions for the boro -tellurite glasses that were prepared. The primary thirteen absorption peaks have been identified at wavelengths of 356, 364, 378, 406, 441, 450, 488, 521, 542, 651, 795, 968, and 1508 nm. The observed spectral bands are associated with the electronic transition from ground state $^4I_{15/2}$ to several excited states, namely $^2G_{7/2}$, $^4G_{9/2}$, $^4G_{11/2}$, $^2H_{9/2}$, $^4F_{3/2}$, $^4F_{5/2}$, $^4F_{7/2}$, $^2H_{11/2}$, $^4S_{3/2}$, $^4F_{9/2}$, $^4I_{9/2}$, $^4I_{11/2}$, and $^4I_{13/2}$, respectively [36]. The transitions, more commonly known as hypersensitive transitions, are governed by certain selection rules: $|\Delta L| \leq 2$, $|\Delta S| = 0$, $|\Delta J| \leq 2$ [36]. As the transitions from $^4I_{15/2}$ to $^2H_{11/2}$, and $^4G_{11/2}$ meet the above criteria [12], these transitions can therefore be classified as hypersensitive. Variation in concentrations of Er^{3+} ions within the host material can result in slight shift in the position of characteristic peaks and the intensity of absorption peaks. Different bonding environments surround Er^{3+} ions, resulting in these variations [37].

The experimental oscillator strength (f_{exp}) was estimated by evaluating the spectral data and Judd-Ofelt (J-O) theory. An expression taken from the literature [38–41] was used to calculate the unified area under

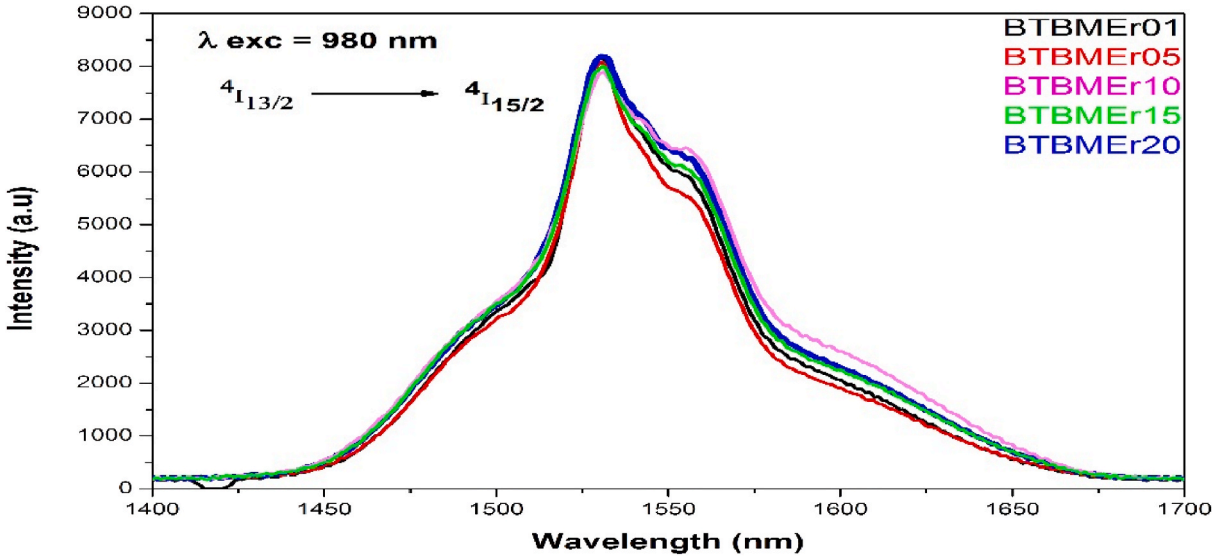

Fig. 7. NIR emission spectra of BTBMEr glasses under excitation of 980 nm diode laser.

Table 5
The Comparison of radiative properties of the transition $^4I_{13/2} \rightarrow {}^4I_{15/2}$ of Er^{3+} ions doped glass with previously reported glasses.

Glass sample	λ_p(nm)	$\tau_{rad\ (ms)}$	A_R (s^{-1})	$\Delta\lambda_{eff}$(nm)	σ_{emi} ($\times 10^{-20}$cm^2)	σ_{emi} x $\Delta\lambda_{eff}$ ($\times 10^{-27}$ cm^3)	σ_{emi} x τ_{rad} ($\times 10^{-24}$ cm^{2}s)	Ref
BTBMEr01	1530	3.161	310.34	74.45	1.541	114.73	48.71	[present work]
BTBMEr05	1530	3.917	255.29	73.52	0.685	50.36	26.83	[present work]
BTBMEr10	1530	3.737	267.55	75.56	1.216	91.88	45.44	[present work]
BTBMEr15	1530	3.777	264.7	79.95	1.412	112.89	53.3	[present work]
BTBMEr20	1530	2.532	394.94	77.45	2.256	174.72	57.12	[present work]
OCBTEr1.0	1536	4.634	215.78	55.4033	0.564	31.25	26.13	[1]
20Te10Er	1532	4.46	224	67	0.90	60.30	40.14	[12]
49S15CfEr1	1535	5.71	175.24	56.32	0.918	51.70	52.42	[18]
SBNCEr05	1530	6.63	306.6	86.89	0.947	82.20	62.79	[20]
PKAlCaFEr10	1536	4.47	224	67	1.05	70.35	46.93	[51]
SANSCEr10	1535	5.18	193	53	0.98	51.94	50.76	[52]
SiPbFEr10	1536	9.4	106.4	60	0.74	44.40	69.56	[53]
BBiLiKEr10	1533	7.05	141.89	81.21	0821	66.67	57.88	[54]

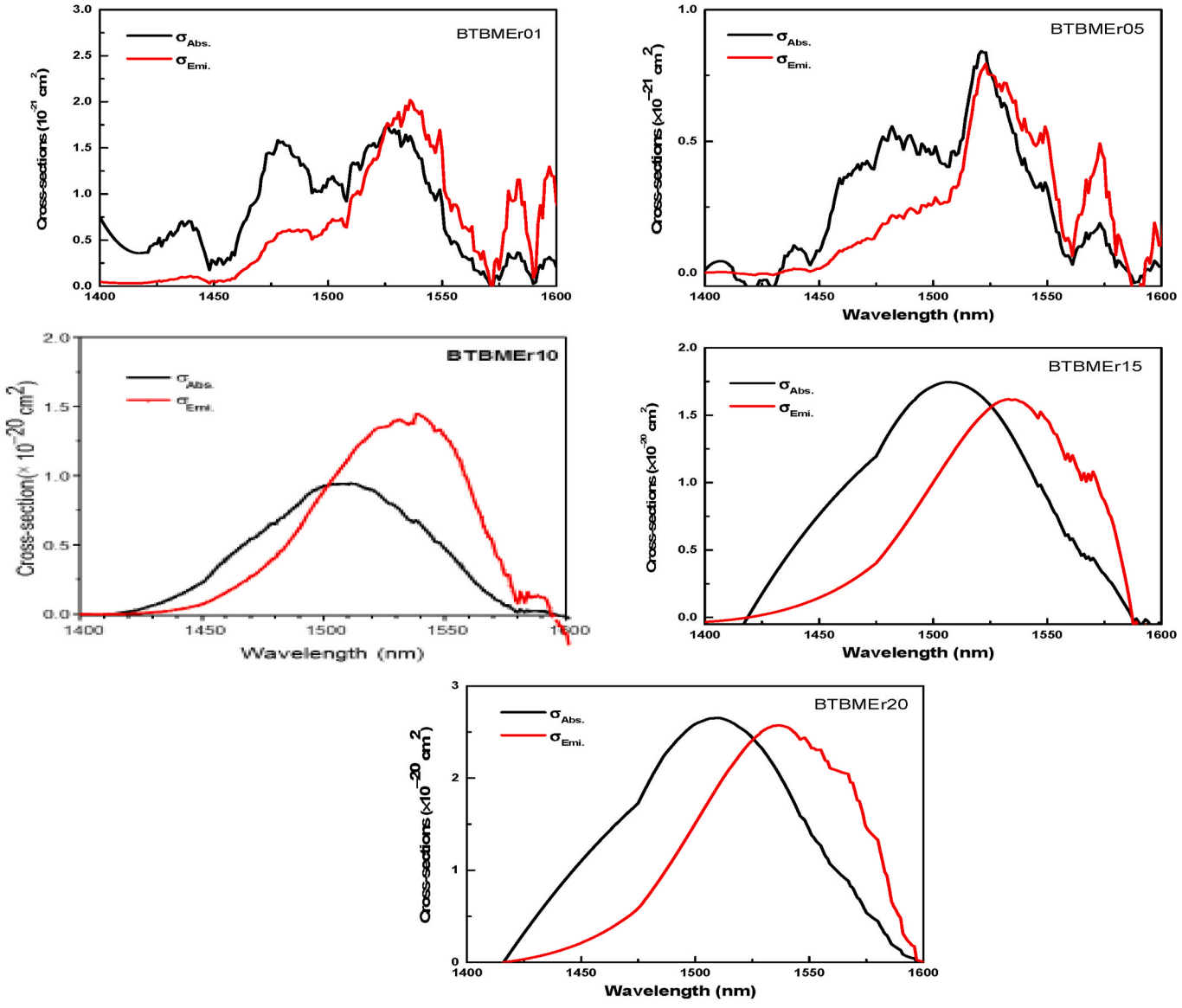

Fig. 8. Absorption and emission cross-section profiles of BTBMEr glasses.

each absorption peak. The calculation of oscillator strength values was carried out based on the expression derived from the existing literature, consistent with the principles of J-O theory [42]. To gauge the level of concordance between the experimentally determined and theoretically computed oscillator strengths, we offer root mean square deviation(rms) values [43]. This metric serves as a measure for assessing the accuracy of the alignment between these two datasets. For each of the prepared samples, we calculated the parameters f_{exp}, f_{cal}, and rms, and these results are presented in Table 3. Notably, in comparison with other transitions, hypersensitive transitions such as $^4I_{15/2}$ to $^2H_{11/2}$, $^4G_{11/2}$

Table 6
Absorption ($^4I_{15/2} \rightarrow {}^4I_{13/2}$) and stimulated emission cross-section ($^4I_{13/2} \rightarrow {}^4I_{15/2}$) values of erbium ions (Er^{3+}) across various materials.

Composition	σ_{emi} ($\times 10^{-20}$ cm^2)	σ_{abs} ($\times 10^{-20}$ cm^2)	Ref.
59.9 B_2O_3– 10TeO_2–15$BaCO_3$–15MgF_2-0.1Er_2O_3	1.751	2.019	**Present Work**
59.5 B_2O_3– 10TeO_2–15$BaCO_3$–15MgF_2-0.5Er_2O_3	0.795	0.842	**Present Work**
59 B_2O_3– 10TeO_2–15$BaCO_3$–15MgF_2–1Er_2O_3	1.408	0.946	**Present Work**
58.5 B_2O_3– 10TeO_2–15$BaCO_3$–15MgF_2-1.5Er_2O_3	1.618	1.745	**Present Work**
58 B_2O_3– 10TeO_2–15$BaCO_3$–15MgF_2–2Er_2O_3	2.571	2.653	**Present Work**
TeO_2–ZnO: Er^{3+} (2 mol %)	0.816	0.881	[57]
74TeO_2–10CdO–15WO_3–Er_2O_3	0.64	0.69	[58]
70TeO_2–20ZnO–10PbO–Er_2O_3–5Yb_2O_3	0.8	0.877	[59]
69.25TeO_2–10ZnF_2–20ZnO–0.75Er_2O_3	0.87	0.957	[60]
15Ga_2O_3–75GeO_2–10Na_2O–0.5Er_2O_3	0.696	0.758	[61]
50P_2O5–30CaO–12Na_2O–Al_2O_3–2AgO–Er_2O_3-4Yb_2O_3	0.6	0.67	[62]
80TeO_2–10BaO–10La_2O_3–Er_2O_3	0.87	0.997	[63]
70TeO_2–5Li_2O–20B_2O_3–5GeO_2: Er_2O_3 (1 wt%), Yb_2O_3 (9 wt%)	0.67	0.77	[64]
75TeO_2–20ZnO–4Na_2O–1Er_2O_3	0.691	0.758	[65]
75TeO_2–20ZnO–3Na_2O–2Er_2O_3	0.345	0.379	[65]

demonstrate elevated values for both f_{exp} and f_{cal}.

The J-O intensity parameters (Ω_2, Ω_4, Ω_6) for prepared BTBMEr glasses were assessed and are provided in Table 4. The aforementioned values have been compared to those found for previously reported erbium-doped materials. Specifically, the Ω_2 values are found to have increased from 6.6678 to 7.9266 $\times 10^{-20}$ cm^2 increment of erbium ions concentration from 0.1 to 2.0 mol % and it followed the trend of $\Omega_2 > \Omega_6 > \Omega_4$. A greater magnitude of Ω_2 indicates a reduction in the level of symmetry in the proximity of Er^{3+} ions. On the other hand, $\Omega_{4,6}$ are linked to the long-range structural arrangement of the host glass, which pertains to the viscosity and stiffness of the glass matrix. For further context, Table 4 provides a comparative analysis of the J-O parameters with the values reported in the existing literature [42–50], offering insights into the distinctive characteristics of the erbium-doped boro-tellurite glasses investigated in this study in relation to existing research. Further spectroscopic quality factor (χ) for all the concentrations were calculated and presented in Table.4. It is used to predict the emissions strengths of various lasing transitions in glass matrix. The decrease in χ value with increase in concentration of erbium ions is related to the quenching of stimulated transition intensities [17].

3.4. NIR emission spectra and radiative parameters

The BTBMEr glass samples were subjected to fluorescence spectroscopy, employing a 980 nm laser diode as the source of excitation within near-infrared region. The resulting spectra are presented in Fig. 7. The observed emission peak at 1530 nm can be ascribed to the transition of erbium ions from $^4I_{13/2}$ to $^4I_{15/2}$. When stimulated by a 980 nm laser, electrons within erbium ions undergo excitation, transitioning from their ground state $^4I_{15/2}$ to their excited state $^4I_{11/2}$ [51]. The process of multiphonon relaxation can enable this energy level to transition into state $^4I_{13/2}$. Consequently, the electrons radiate back to their ground state, producing strong emission at 1530 nm in the process. It is of significance to observe that, in the present work, the near-infrared (NIR) emission peak remains unchanged as the concentration of erbium ions increases. However, the intensity slightly changes with concentrations, accompanied by a broadening of the spectral range.

Analyzing the spectroscopic characteristics of a host matrix is essential for finding suitable active lasing media and broadband amplifiers. In this context, we have evaluated radiative characteristics, encompassing specific parameters such as radiative life time (τ_{rad}), emission peak position (λ_p), effective bandwidth ($\Delta\lambda_{eff}$), radiative transition probability (A_R), stimulated emission cross-section (σ_{emi}), optical gain ($\sigma_{emi} \times \tau_{rad}$) and gain bandwidth ($\sigma_{emi} \times \Delta\lambda$eff). For our investigation, we focused on evaluating the radiative properties associated with the transition from $^4I_{13/2} \rightarrow {}^4I_{15/2}$ of Er^{3+} ions embedded in boro-tellurite glasses. The findings of this study have been documented in Table 5 and a comparative analysis has been conducted with the previously published results [52–55]. The examination of Table.5 indicates that the BTBMEr20 glass specimen demonstrates the highest emission cross-section, measuring 2.256 $\times 10^{-20}$ cm^2, and key parameters such as $\Delta\lambda_{eff}$ of 77.45 nm, gain bandwidth of 111.73 $\times 10^{-27}$ cm^3, and optical gain of 57.12 $\times 10^{-24}$ cm^2s. These results indicate that the BTBMEr20 glass sample holds great promise as a candidate for amplification processes at a wavelength of 1.53 μm.

3.5. Mc-Cumber theory and gain cross-section profiles

The evaluation of absorption cross-section (σ_{abs}) for the transition $^4I_{15/2}$ to $^4I_{13/2}$ of erbium ions in all the prepared samples is obtained from the following equation:

$$\sigma\text{abs}(\lambda) = 2.303 \frac{\boldsymbol{OD}(\boldsymbol{\lambda})}{\boldsymbol{Nl}} \quad (2)$$

the symbol OD (λ) corresponds to the optical density, variable N denotes the erbium ions concentration within the glass, while ***l*** specifies the thickness of the glass specimen. Following the Mc-Cumber theory, we performed the computation of stimulated emission cross-section (σ_{emi}) for laser transitions from $^4I_{13/2}$ to $^4I_{15/2}$ across all specimens. The subsequent equation was employed for this purpose.

$$\sigma_{emi}(\lambda) = \sigma_{abs}(\lambda) \exp\left(\frac{\boldsymbol{\varepsilon} - \boldsymbol{hc}\lambda^{-1}}{\boldsymbol{kT}}\right) \quad (3)$$

Here the symbol $\sigma_{abs}(\lambda)$ represents absorption cross section, ***h*** marks the Planck constant, ***k*** denotes Boltzmann constant, while the parameter ε represents the minimum amount of free energy required for the transition of erbium ions from $^4I_{13/2}$ to $^4I_{15/2}$ at a specific temperature T. Determination of ε can be accomplished using the methodology outlined in Ref. [56]. Fig. 8 illustrates the wavelength dependent trends of $\sigma_{abs}(\lambda)$, $\sigma_{emi}(\lambda)$ during the transition from $^4I_{13/2}$ to $^4I_{15/2}$ across all the glass compositions that were prepared. A subsequent comparison of these findings with data from alternative laser materials is detailed in Table 6.

The profiles of gain cross-section (G) were acquired by employing the designated relationship as defined below [20]:

$$G(\lambda, \gamma) = \boldsymbol{\gamma\sigma_{emi}}(\boldsymbol{\lambda}) - (1-\gamma)\boldsymbol{\sigma_{abs}}(\boldsymbol{\lambda}) \quad (4)$$

The parameter γ denotes the population inversion, which signifies the correlation between the erbium ions concentration specifically located at the lasing level $^4I_{13/2}$ and the total erbium ions concentration existing in the glass material. Using previously computed values of $\sigma_{emi}(\lambda)$, $\sigma_{abs}(\lambda)$ and considering a range of γ values from 0 to 1 with an interval of 0.2, the profiles of gain cross-section were obtained for all the glass samples and are depicted in Fig. 9.

Observations from Fig. 9 reveal that the gain cross section becomes positive when γ exceeds 0.5, reaching its peak at $\gamma = 1$ for all the samples. Notably, the BTBMEr20 sample demonstrates the highest gain cross-section value, measuring 2.571 $\times 10^{-20}$ cm^2. Additionally, a significant positive gain response is observed in the wavelength ranges of 1460–1530 nm (S band) and 1530–1565 nm (C band) This suggests the potential application of these samples as optical amplifiers within the S + C communication window [12].

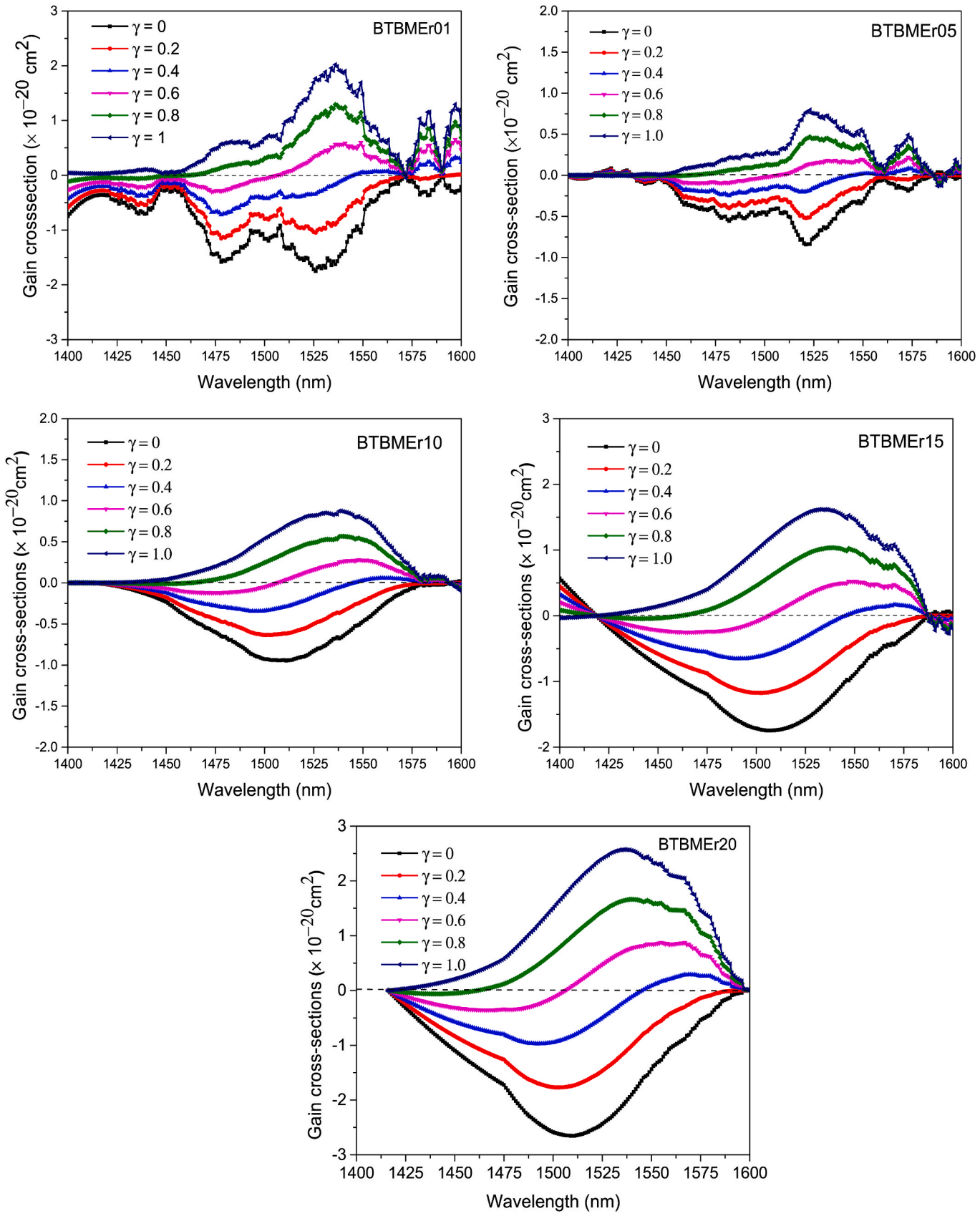

Fig. 9. Gain cross-section profiles of $^4I_{13/2} \rightarrow {}^4I_{15/2}$ transition of Er-doped telluroborate glasses.

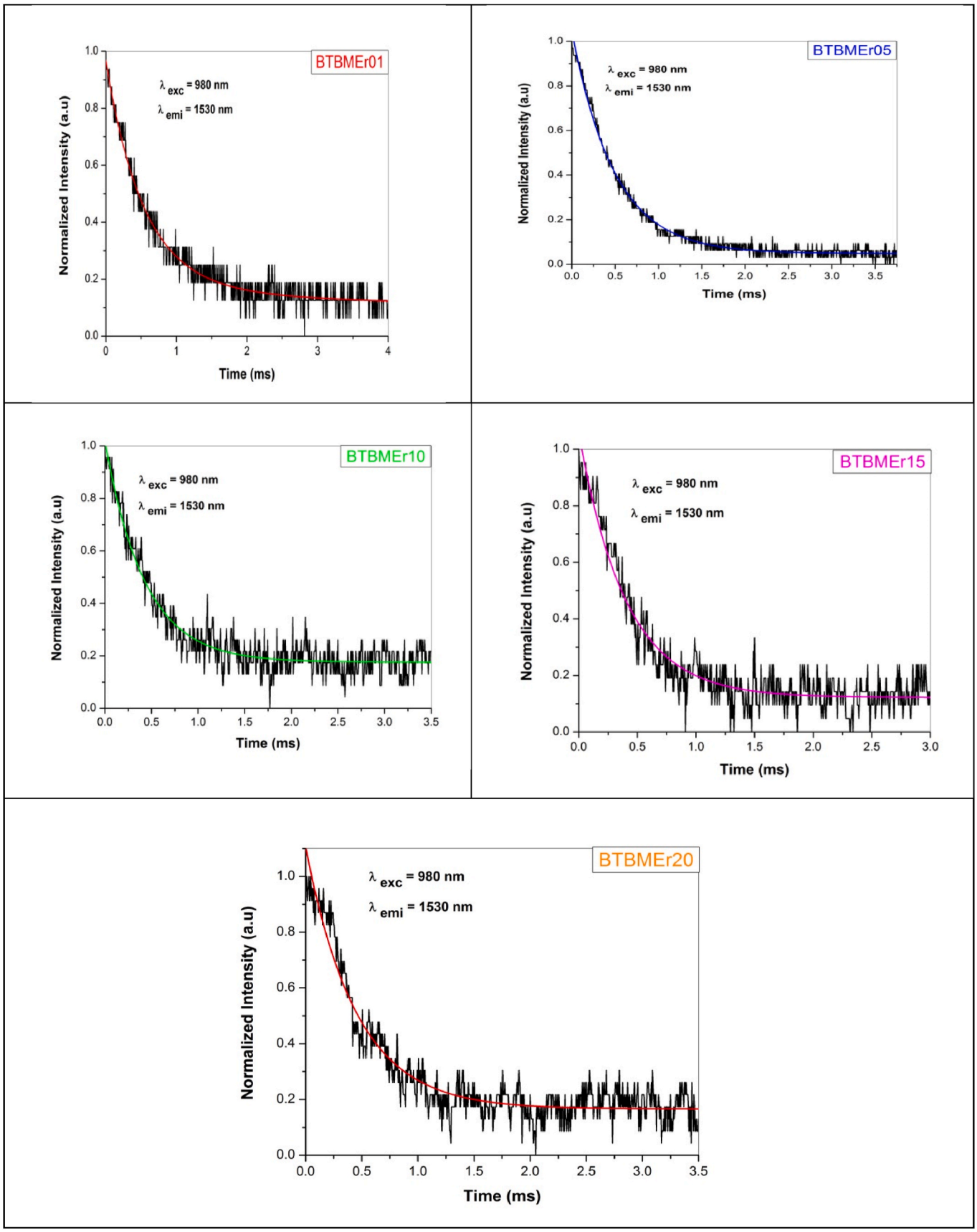

Fig. 10. Photoluminescence decay curves of $^4I_{13/2} \rightarrow {}^4I_{15/2}$ transition under 980 nm laser excitation of Er-doped borotellurite glasses.

Table 7
Comparison of fluorescence lifetime of $^4I_{13/2}$ excited level of Er^{3+} ions in BTBMEr glasses with erbium-doped other glasses.

Sample	τ_{exp}(ms)	Ref
BTBMEr01	2.453	Present Work
BTBMEr05	3.215	Present Work
BTBMEr10	3.141	Present Work
BTBMEr15	3.254	Present Work
BTBMEr20	2.356	Present Work
20Te0.5Er	0.525	[12]
20Te1Er	0.315	[12]
20Te2Er	0.234	[12]
20Te4Er	0.094	[12]
SBNCEr0.05	6.94	[20]
SBNCEr01	6.61	[20]
SBNCEr05	5.46	[20]
SBNCEr10	5.44	[20]
SBNCEr20	2.74	[20]
LBBPE01	1.04	[28]
LBBPE03	1.01	[28]
LBBPE05	0.90	[22]
Er:SrTP	0.402	[56]
Er:MgTP	0.360	[56]
Er:CaTP	0.338	[56]

3.6. Decay lifetime analysis

Fig. 10. Showcases the fluorescence decay profiles of Er^{3+} ions doped glass samples. These decay curves were observed at a wavelength of 980 nm for excitation and a wavelength of 1530 nm for emission. To analyze the decay curves, a second-order exponential decay model was employed, which can be expressed as

$$I(t) = I_0 + A_1 e^{-t/\tau_1} + A_2 e^{-t/\tau_2} \quad (5)$$

In this equation, I(t) represents luminescence intensity at a given time t, additionally τ_1,τ_2 refers short and long decay components, while A_1,A_2 are used as the corresponding intensity coefficients, while I_0 is used to denote the background intensity [66].

The experimental lifetime τ_{exp}, is determined by employing the following relationship

$$\tau_{exp} = \frac{A_1\tau_1^2 + A_2\tau_2^2}{A_1\tau_1 + A_2\tau_2} \quad (6)$$

The τ_{exp} values that are determined that were determined are in Table 7. The τ_{exp} data demonstrate a decrease from 1.0 ms to 0.40 ms, indicating a concurrent rise in the erbium ions concentration from 0.5 to 1.5 mol%. The decrease in the measured duration can be attributed to non-radiative mechanisms such as multiphonon relaxation, cross relaxation between pairs of erbium ions which can be understand through partial energy level diagram depicted in Fig. 11. Once the concentration exceeds 1.5 mol%, the τ_{exp} values begins to rise. This increase is believed to be caused by the interplay among the stimulated Er^{3+} ions. This pattern aligns with observations made in other glasses doped with Er^{3+} ions [17,22,30,67].

4. Conclusions

In this study, we have explored erbium-doped boro-tellurite glasses for potential optoelectronic devices. A thorough investigation was conducted of the glasses' physical, structural, thermal, and spectroscopic properties. We conducted X-ray diffraction and EDX analyses on the prepared samples, revealing their amorphous nature, excellent thermal stability, and structural rigidity. Identification of functional groups in the samples was accomplished using FTIR spectroscopy. The Judd-Ofelt parameters exhibited intriguing variations, with the BTBMEr20 glass showcasing the greatest values ($\Omega_2 = 7.926 \times 10^{-20}$ cm^2, $\Omega_4 = 2.57 \times 10^{-20}$ cm^2 and $\Omega_6 = 3.62 \times 10^{-20}$ cm^2). Under 980 nm laser excitation, NIR emission spectra spanning 1400–1600 nm were measured and the radiative characteristics of the 1530 nm peak pertaining to the transition from $^4I_{13/2}$ to $^4I_{15/2}$ of erbium ions were evaluated. BTBMEr20 glass sample highlighted with an effective bandwidth ($\Delta\lambda_{eff}$) of 77.45 nm, gain bandwidth of 114.73×10^{-27} cm^3, and optical gain of 57.12×10^{-24} cm^2s. The prepared samples were also subjected to a photoluminescence decay analysis, offering valuable insights. The results suggest that BTBMEr20 glass holds promise as a possible candidate for enhancing and amplifying optical signals at a wavelength 1.53 μm.

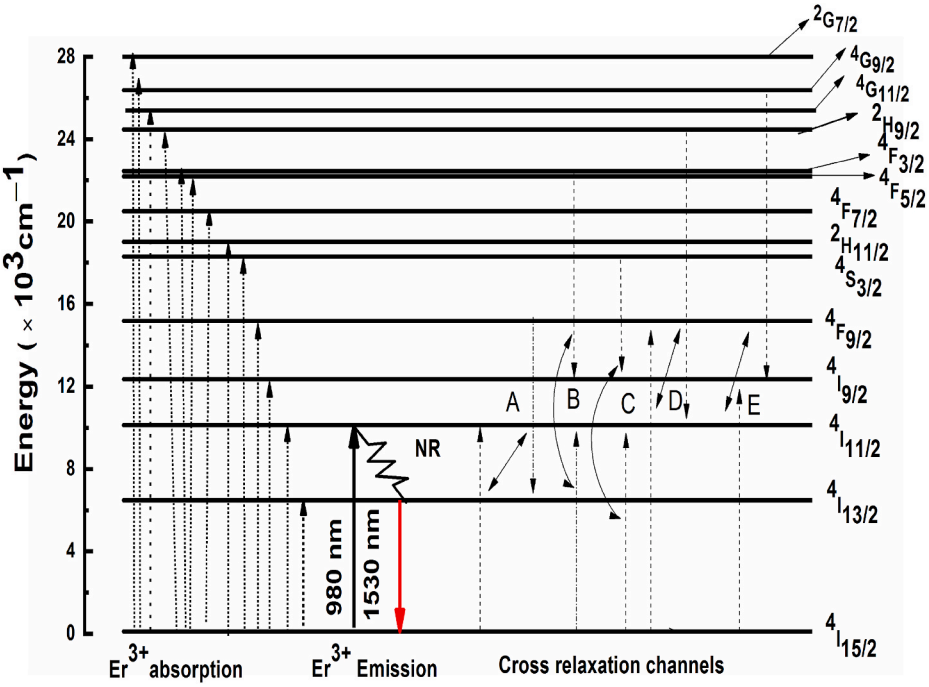

Fig. 11. Partial energy level diagram of $^4I_{13/2} \rightarrow {}^4I_{15/2}$ transition under 980 nm laser excitation of Er-doped borotellurite glasses.

CRediT authorship contribution statement

B. Kiran Kumar: Writing – original draft. **P. Reddi Babu:** Conceptualization. **Esra Kavaz:** Data curation. **Yuwaraj K. Kshetri:** Formal analysis. **Tae-Ho Kim:** Methodology. **Virgilio de Carvalho dos Anjos:** Resources. **B. Deva Prasad Raju:** Formal analysis.

Declaration of competing interest

A series of glass compositions (60-x) B_2O_3–10TeO_2–15$BaCO_3$–15MgF_2–xEr_2O_3 with varying concentrations of erbium ions (Er^{3+}) was synthesized using the melt quenching technique and the samples were subjected to thorough characterization to explore their optical and structural properties. To validate the amorphous nature of the glass and gain insights into their chemical bonds, standard characterization techniques such as X-ray diffraction and Fourier transform infrared spectroscopy were employed. The absorption spectra of the Er^{3+} doped glasses were used to calculate the Judd-Ofelt intensity parameters, providing valuable information about the local environment and coordination of Er^{3+} ions within the glass matrix. Near-infrared (NIR) emission spectra were acquired for these glasses containing Er^{3+} ions and their spectral characteristics, emission cross-section, and gain-coefficient parameters were analyzed. These spectra revealed distinctive features, including a prominent NIR band corresponding to the $^4I_{13/2} \rightarrow {}^4I_{15/2}$ transition centered at 1530 nm. This emission band spanned the wavelengths commonly used in optical communication systems, including the S-, C-, and L-bands, making these glasses suitable candidates for applications such as wavelength division multiplexing (WDM). These results suggest that the boro-tellurite glass may have potential use in photonic devices designed for near-infrared applications, including optical communication systems.

We believe that our findings results could be of interest to the readers of scientific community. The article will be highly useful to future research on the subject; we hope that the editorial board and the reviewers will agree on the interest of this study.

Data availability

Data will be made available on request.

Acknowledgement

The characterization facility was supported by Brain Pool Program through the National Research Foundation of Korea funded by the Ministry of Science and ICT (Grant No.2020H1D3A1A02081359) as well as Basic Science Research Program through the National Research Foundation of Korea funded by the Ministry of Education (Grant No.2021R1I1A3059543).

References

[1] R.A.A. Silva, N.F. Dantas, R.F. Muniz, A.M.O. Lima, F. Pedrochi, A. Steimacher, M. J. Barboz, Optical and spectroscopic properties of Er3+/Yb3+ co-doped calcium borotellurite glasses, J. Lumin. 251 (2022) 119239, https://doi.org/10.1016/j.jlumin.2022.119239.

[2] Yin Zhang, Wei Zhu, Hao Xu, Yubo Wu, Yuhan Zou, Spectroscopic properties of Er3+/Yb3+ co-doped fluoro bismuth borate glasses for up-conversion luminescence, J. Non-Cryst. Solids 599 (2023) 121963, https://doi.org/10.1016/j.jnoncrysol.2022.121963.

[3] G. Lakshminarayana, M.I. Sayywd, S.O. Baki, A. Lira, M.G. Dong, Kawa M. Kaky, I. V. Kityk, M.A. Mahdi, Optical absorption and gamma-radiation-shielding parameter studies of Tm^{3+} - doped multicomponent borosilicate glasses, Appl. Phys. A 124 (2018) 378, https://doi.org/10.1007/s00339-018-1801-4.

[4] Kawa M. Kaky, Erdem Sakar, Ugur Akbaba, A. Emre Kasapoglu, M.I. Sayyed, Emre Gur, S.O. Baki, M.A. Mahdi, X-ray photoelectron spectroscopy (XPS) and gamma-ray shielding investigation of boro-silicate glasses contained alkali/alkaline modifier, Results Phys. 14 (2019) 102438, https://doi.org/10.1016/j.rinp.2019.102438.

[5] M.H.A Mhareb, Muna Alqahtani, Y.S. Alajerami, Fatimh Alshahri, M.I. Sayyed, K.A. Mahmoud, Noha Saleh, N.Alonizan, M.S. Al-Buriahi, Kawa M. Kaky, Ionizing radiation shielding features for titanium borosilicate glass modified with different concentrations of barium oxide, Mater. Chem. Phys. 272 (2021) 125047,https://doi.org/10.1016/j.matchemphys.2021.125047.

[6] G.Lakshminarayana, Kawa M.Kaky, J.J edryka, A.M. El-Naggar, A.A. Albassam, G. Myronchuk, M.A. Mahdi, Laer induced elastooptics in novel Bi2O3, and Pr2O3 doped tellurite rich glasses, Mater. Lett., 183,322-324, https://doi.org/10.1016/j.matlet.2016.07.129.

[7] Kawa M. Kaky, M.I. Sayyed, Selected germanate glass systems with robust physical features for radiation protection material use, Radiat. Phys. Chem. 215 (2024) 111321, https://doi.org/10.1016/j.radphyschem.2023.111321.

[8] G.V. Jagadeesha Gowda, C. Devaraja, B. Eraiah, A. Dahshan, S.N. Nazrin, Structural, thermal and spectroscopic studies of Europium trioxide doped lead boro-tellurite glasses, J. Alloys Compd. 871 (2021) 159585, https://doi.org/10.1016/j.jallcom.2021.159585.

[9] E.S. Nurbaisyatul, K. Azman, H. Azhan, W.A.W. Razali, A. Noranizah, S. Hashim, Y. S.M. Alajerami, The optical properties of trivalent rare earth ions (Er^{3+}) doped borotellurite glass, Opt Spectrosc. 116 (2014) 413–415, https://doi.org/10.1134/S0030400X14030163.

[10] M Amar Kumar, T. Sankarappa, J.S. Ashwajeet, T. Sujatha, Polaron conduction mechanisms in (B_2O_3)-(TeO_2)-(MoO_3)- (Er_2O_3) glasses, J. Phys. Conf. 1172 (2019) 012012, https://doi.org/10.1016/j.matpr.2019.07.559.

[11] Joao Coelho, Joao Azevedo, Hungerford Graham, N. Sooraj Hussain, Luminescence and decay trends for NIR transition ($^4I_{13/2}$ to $^4I_{15/2}$) at 1.5 μm in Er^{3+} doped LBT glasses, Opt. Mater. 33 (2011) 1167–1173, https://doi.org/10.1016/j.optmat.2011.02.003.

[12] Nimitha S. Prabhu, A.N. Meza-Rocha, O. Soriano-Romero, U. Caldino, E.F. Huerta, C. Falcony, M.I. Sayyed, Hanan Al-Ghamdi, Aljawhara H. Almuqrin, Sudha D. Kamath, Spectroscopic study of Er^{3+} doped borate glass system for green emission device, NIR laser, and optical amplifier applications, J. Lumin. 238 (2021) 118216, https://doi.org/10.1016/j.jlumin.2021.118216.

[13] V. Murali Krishna, Sk Mahamuda, Rupesh A. Talewar, K. Swapna, M. Venkateswarlu, A.S. Rao, Rajesh, Dy^{3+} ions doped oxy-fluoroboro tellurite glasses for the prospective optoelectronic device applications, J. Alloys Compd. 762 (2018) 814–826, https://doi.org/10.1016/j.jallcom.2018.05.191.

[14] Kenji Shinozaki, Sohei Sukenaga, Hiroyuki Shibata, Tomoko Akai, Effect of Mg^{2+} and fluorine on the network and highly efficient photoluminescence of Eu^{3+} ion in MgF_2–BaO–B_2O_3 glasses, J. Am. Ceram. Soc. 102 (2019) 2531–2541, https://doi.org/10.1111/jace.16165.

[15] P. Sailaja, Sk Mahamuda, K. Swapna, M. Venkateswarlu, Mohini Gupta, A.S. Rao, Broadband NIR emission at 1.53 μm in trivalent erbium ions doped SrO-Al_2O_3-B_2O_3-$BaCl_2$-10TeO_2 glasses for optical fiber and NIR laser applications, J. Non-Cryst. Solids 567 (2021) 120937, https://doi.org/10.1016/j.jnoncrysol.2021.120937.

[16] K. Selvaraju, K. Marimuthu, Structural and spectroscopic studies on Er^{3+} doped boro tellurite glasses, Physica B 407 (2012) 1086–1093, https://doi.org/10.1016/j.physb.2012.01.003.

[17] N.L. Amiar Rodin, M.R. Sahar, Erbium doped sodium magnesium boro-tellurite glass: stability and JuddOfelt analysis, Mater. Chem. Phys. 216 (2018) 177–185, https://doi.org/10.1016/j.matchemphys.2018.06.006.

[18] G. Lakshminarayana, Kawa M. Kaky, S.O. Baki, A. Lira, Priyanka Nayar, I.V. Kityk, M.A. Mahdi, Physical, structural, thermal, and optical spectroscopy studies of TeO_2-B_2O_3-MoO_3-ZnO-R_2O (R = Li, Na, and K)/MO (M= Mg, Ca, and Pb) glasses, J. Alloys Compd. 690 (2017) 799e816, https://doi.org/10.1016/j.jallcom.2016.08.180.

[19] S. L. Meena and Beena Bhatia, Polarizability and Optical Basicity of Er^{3+} Ions Doped Zinc Lithium Bismuth Borate Glasses, J. Pure Appl. Ind. Phys., Vol.6(10), 175-183, ISSN 0976-5727 (Print) ISSN 2319-8133 (Online) https://doi.org/10.9790/4861-0804044954.

[20] Megala Rajesh, M. Reddi Babu, N. John Sushma, B. Deva Prasad Raju, Influence of Er^{3+} ions on structural and fluorescence properties of SiO_2- B_2O_3- Na_2CO_3-NaF-CaF_2 glasses for broadband 1.53μm optical amplifier applications, J. Non-Cryst. Solids, 119732. https://doi.org/10.1016/j.jnoncrysol.2019.119732,.

[21] K. Linganna, D. Viswanath, R. Narro-Garcia, S. Ju, W.-T. Han, C.K. Jayasankar, V. Venkatramu, Thermal and optical properties of Nd^{3+} ions in K- Ca-Al fluorophosphate glasses, J. Lumin. 166 (2015) 328–334, https://doi.org/10.1016/j.jlumin.2015.05.024.

[22] G. Devarajulu, G. Lakshminarayana, P. Venkateswara Rao, Dong-Eun Lee, Jonghun Yoon, Taejoon Park, Er^{3+}-doped SiO_2-based glasses – an exploration of structural, visible, chromatic, and NIR fluorescence characteristics, Mater. Res. Bull. 147 (2022) 111634, https://doi.org/10.1016/j.materresbull.2021.111634.

[23] P. Suthanthirakumar, P. Karthikeyan, P.K. Manimozhi, K. Marimuthu, Structural and spectroscopic behavior of Er^{3+}/Yb^{3+} co-doped boro-tellurite glasses, J. Non-Cryst. Solids 410 (2015) 26–34, https://doi.org/10.1016/j.jnoncrysol.2014.12.012.

[24] Kawa M. Kaky, M.I Sayyed, Abbas Khammas, Ashok Kumar, Erdem Sakar, Alyaa H. Abdalsalam, Betul Ceviz Sakar, Bunyamin Alim, M.H.A. Mhareb, Theoretical and experimental validation gamma shielding properties of B_2O_3-ZnO-MgO-Bi_2O_3 glass system, Mater. Chem. Phys., 122504,https://doi.org/10.1016/j.matchemphys.2019.122504.

[25] Ibrahim Bulus, R. Hussin, S.K. Ghoshal, Abd R. Tamuri, S.A. Jupri, Enhanced elastic and optical attributes of boro-telluro-dolomite glasses: role of CeO_2 doping, Ceram. Int. 45 (2019) 18648–18658, https://doi.org/10.1016/j.ceramint.2019.06.089.

[26] K. Siva Rama Krishna Reddy, K. Swapna, Sk Mahamuda, M. Venkateswarlu, A. S. Rao, Structural, optical and photoluminescence properties of alkaline-earth boro tellurite glasses doped with trivalent Neodymium for 1.06 μm optoelectronic

devices, Opt. Mater. 111 (2021) 110615, https://doi.org/10.1016/j.optmat.2020.110615.
[27] Zahra Ashur Said Mahraz, E.S. Sazali, M.R. Sahar, Spectral and dielectric characteristics of Er^{3+} doped multicomponent tellurite glasses, Optik 239 (2021) 166776, https://doi.org/10.1016/j.ijleo.2021.166776.
[28] K. Keshavamurthy, B. Eraiah, Er^{3+} Ions doped alkali boro bismuth tellurite glasses for photonic applications, AIP Conf. Proc. 2142 (2019) 050010, https://doi.org/10.1063/1.5122376.
[29] Sangeeta, B. Kolavekar, and N.H. Ayachit, Thermal Properties of Pr_2O_3 Doped Lead Boro-Tellurite Glasses, International Conference on Multifunctional Materials, AIP Conf. Proc. 2269, 030070-1–030070-5;https://doi.org/10.1063/5.0019594.
[30] A. Madhu, B. Eraiah, P. Manasa, Ch Basavapoornima, Er^{3+} ions doped lithium-bismuth-boro-phosphate glass for 1532 nm emission and efficient red emission up conversion for telecommunication and lasing applications, J. Non-Cryst. Solids 495 (2018) 35–46, https://doi.org/10.1016/j.jnoncrysol.2018.04.060.
[31] Yang Yanmin, Liu Yanzhou, Cai Peiqing, RamziMaalej, HyoJinSeo, Thermal stability and spectroscopic properties of Ho^{3+} doped tellurite-borate glasses, J. Rare Earths, 33 (9), 939-945.https://doi.org/10.1016/S1002-0721(14)60509-3.
[32] P. Suthanthirakumar, S. Arunkumar, K. Marimuthu, Spectroscopic properties and Excited state dynamics of Sm^{3+} ions in Zinc telluro-fluoroborate glasses, J. Lumin., 202, 289-300. https://doi.org/10.1016/j.jlumin.2018.05.069,.
[33] Kawa M. Kaky, G.Lakshminarayana, S.O. Baki, M.K. Halimah, M.A. Mahdi, Structural, Thermal and Optical Studies of Bismuth doped multicomponent Telllurite Glass, Solid State Phenom., 268, 165-171, https://doi.org/10.4028/www.scientific.net/SSP.268.165.
[34] Kawa M. Kaky, M.I. Sayyed, M.H.A. Mhareb, Haider H. Abbas, S. Baki, Physical, structural, mechanical, and various radiation shielding properties of TeO2-GeO2-ZnO-Al_2O_3-Li_2O_3-M (M= WO_3, MoO_3, PbO, and CuO) glasses, Opt. Mater. 145 (2023) 114370, https://doi.org/10.1016/j.optmat.2023.114370.
[35] Kawa M. Kaky, M.I. Sayyed, Farah Laariedh, Alyaa H. Abdalsalam, H.O. Tekin, S. O. BakStuctural, Optical and radiation shielding properties of zinc borotellurite alumina glasses, Appl. Phys. A 125 (2019) 32, https://doi.org/10.1007/s00339-018-2329-3.
[36] Weiwei Ma, Liangbi Su, Xiaodong Xu, Jingya Wang, Dapeng Jiang, Lihe Zheng, Xiuwei Fan, Chun Li,Jie Liu, and Jun Xu, Effect of erbium concentration on spectroscopicproperties and 2.79 μm laser performance of Er:CaF_2 crystals, Opt. Mater. Express, 6(2), 409.https://doi.org/10.1364/OME.6.000409.
[37] Umar Saad Aliyu, Halimah Mohamed Kamari, Ibrahim GanaGeidam, Ibrahim OlanrewajuAlade, Azlan Muhammad Noorazlan, Abdulkarim Muhammad Hamza, Ahmad Fahad Ahmad, Spectroscopic investigations of Er_2O_3 doped silica borotellurite glasses, Opt. Mater. 114 (2021) 110987, https://doi.org/10.1016/j.optmat.2021.110987.
[38] M. J Weber, Probabilities for Radiative and Nonradiative Decay of Er^{3+} in LaF_3, Phys. Rev., 157(2), 262–272. https://doi.org/10.1103/physrev.157.262.
[39] Markus P. Hehlen, Mikhail G. Brik, Karl W. Kramer, 50th anniversary of the Judd–Ofelt theory: An experimentalist's view of the formalism and its application. 136, 221-239, https://doi.org/10.1016/j.jlumin.2012.10.035.
[40] G.S. Oflet, Intensities of crystal spectra of RareEarth ions, J. Chem. Phys. 37 (1962) 511, https://doi.org/10.1063/1.1701366.
[41] B.R. Judd, Optical absorption intensities of rare-earth ions, Phys. Rev. 127 (1962) 750, https://doi.org/10.1103/PhysRev.127.750.
[42] T. Sasikala, L. Rama Moorthy, A. Mohan Babu, Optical and luminescent properties of Sm^{3+} doped tellurite glasses, Spectrochim. Acta Mol. Biomol. Spectrosc. 104 (2013) 445–450, https://doi.org/10.1016/j.saa.2012.11.088.
[43] Kawa M. Kaky Mustafa Dh Hassib, Ashok Kumar, Erdem Sakar, M.I. Sayyed, S. O. Baki, M.A. Mahdi, Boro-silicate glasses co-doped Er3+/Yb3+ for optical amplifier and gamma radiation shielding applications, Phys. B Condens. Matter 567 (2019) 37–44, https://doi.org/10.1016/j.physb.2019.05.006.
[44] Tirtha Som, Basudeb Karmakar, Nephelauxetic effect of low phonon antimony oxide glass in absorption and photoluminescence of rare-earth ions, Spectrochim. Acta Mol. Biomol. Spectrosc. 79 (2011) 1766–1782, https://doi.org/10.1016/j.saa.2011.05.054.
[45] Fang Ren, M.E.I. Yu-zhao, Chao Gao, Li-gang Zhu, LU An-xian, Thermal stability and Judd-Ofelt analysis of optical properties of Er^{3+} doped tellurite glasses, Trans. Nonferrous Metals Soc. China 22 (2012) 20212026, https://doi.org/10.1016/S1003-6326(11)61423-4.
[46] L.R. Moorthy, M. Jayasimhadri, S.A. Saleem, D.V.R. Murthy, Optical properties of Er^{3+} doped alkali fluorophosphate glasses, J. Non-Cryst. Solids 353 (2007) 1392–1396, https://doi.org/10.1016/j.jnoncrysol.2006.10.062.
[47] B. Jamalaiah, T. Suhasini, L.R. Moorthy, K.J. Reddy, I.-G. Kim, D.-S. Yoo, K. Jang, Visible and near infrared luminescence properties of $Er3^+$ doped LBTAF glasses for optical amplifiers, Opt. Mater. 34 (2012) 861–867, https://doi.org/10.1016/j.optmat.2011.11.023.
[48] K. Mariselvam, Juncheng Liu, A novel Er^{3+} ions doped zirconium magnesium borate glass with very high quantum efficiency for green laser and optical amplifier applications, Solid State Sci., 111 (2021), 106443, https://doi.org/10.1016/j.solidstatesciences.2020.106443..
[49] Ch Basavapoornima, K. Linganna, C.R. Kesavulu, S. Ju, B.H. Kim, W.T. Han, C. K. Jayasankar, Spectroscopic and pump power dependent upconversion studies of Er^{3+} doped lead phosphate glasses for photonic applications, J. Alloys Compd. 699 (2017) 959–968, https://doi.org/10.1016/j.jallcom.2016.12.199.
[50] K. Annapoorani, Ch Basavapoornima, N. Suriya Murthy, K. Marimuthu, Investigations on structural and luminescence behavior of Er^{3+} doped Lithium Zinc borate glasses for lasers and optical amplifier applications, J. Non-Cryst. Solids 447 (2016) 273–282, https://doi.org/10.1016/j.jnoncrysol.2016.06.021.
[51] J.F. Gomes, A.M.O. Lima, M. Sandrini, A.N. Medina, A. Steimacher, F. Pedrochi, M. J. Barboza, Optical and spectroscopic study of erbium doped calcium borotellurite glasses, Opt. Mater. 66 (2017) 211e219, https://doi.org/10.1016/j.optmat.2017.02.010.
[52] S. NayabRasool, B.C. Jamalaiah, K. Suresh, L. Ramamoorthy, C.K. Jayasankar, Spectroscopic properties of Er^{3+} -doped phosphate based glasses for broadband 1.54 μm emission, J. Mol. Struct. 1130 (2017) 837–843, https://doi.org/10.1016/j.jlumin.2017.10.072.
[53] G. Devarajulu, O. Ravi, C.M. Reddy, S.Z. Ali Ahamed, B Deva Prasad Raju, Spectroscopic properties and upconversion studies of Er^{3+} doped SiO_2-Al_2O_3-Na_2CO_3-SrF_2-CaF_2 oxyfluoride glasses for optical amplifier applications, J. Lumin. 194 (2018) 499–506, https://doi.org/10.1016/j.jlumin.2017.10.072.
[54] S. Xu, Z. Yang, S. Dai, J. Yang, L. Hu, Z. Jiang, Spectral properties and thermal stability of Er-doped oxyfluoride silicate glasses for broadband optical amplifier, J. Alloys Compd. 361 (2003) 313–319, https://doi.org/10.1016/S0925-8388(03)00447-X.
[55] M. Mariyappan, S. Arunkumar, K. Marimuthu, Judd-Ofelt analysis and NIR luminescence investigations on Er^{3+} ions doped B_2O_3–Bi_2O_3–Li_2O–K_2O glasses for photonic applications, Phys. B 572 (2019) 27–35, https://doi.org/10.1016/j.physb.2019.07.036.
[56] Y. Benmadani, A. Kermaoui , M. Chalal , W. Khemici , A. Kellou , F. Pelle, Erbium doped tellurite glasses with improved thermal properties as promising candidates for laser action and amplification, Opt. Mater. 35(120 22434-2240 , https://doi.org/10.1016/j.optmat.2013.06.014,.
[57] N. Jaba, H. Ben Mansour, A. Kanoun, A. Brenier, B. Champagnon, Spectral broadening and luminescence quenching of 1.53 mm emission in Er^{3+} doped zinc tellurite glass, J. Lumin. 129 (2009) 270–276, https://doi.org/10.1016/j.jlumin.2008.10.006.
[58] G. Bilir, G. Ozen, D. Tatar, M.L. Ovecoglu, Judd–Ofelt analysis and near infrared emission properties of the Er^{3+} ions in tellurite glasses containing WO_3 and CdO, Opt Commun. 284 (2011) 863–868. https://doi:10.1016/j.optcom.2010.09.087.
[59] Zhe Jin, Qiuhua Nie, Tiefeng Xu, Shixun Dai, Xiang Shen, Xianghua Zhang, Optical transitions and upconversion luminescence of Er^{3+}/Yb^{3+} codoped lead–zinc–tellurite oxide glass, Mater. Chem. Phys. 104 (2007) 62–67, https://doi.org/10.1016/j.matchemphys.2007.02.071.
[60] E.F. Chillcce, I.O. Mazali, O.L. Alves, L.C. Barbosa, E.F. Chillcce, Optical and physical properties of Er^{3+}-doped oxy-fluoride tellurite glasses, Opt. Mater. 33 (2011) 389–396, https://doi.org/10.1016/j.optmat.2010.09.027.
[61] D.M. Shi, Y.G. Zhao, X.F. Wang, Enhanced 1.53-μm and lowered upconversion luminescence in Er^{3+}-doped Ga_2O_3–GeO_2–Bi_2O_3–Na_2O glass by codoping rare earths , Physica B 406 (13) 2588–2593, doi:10.1016/j.physb.2011.03.074.
[62] Chengguo Ming, Feng Song, Yu Yin, Gong Zhang, Qingru Wang, Hua Yu, Tongqing Sun, Jianguo Tian, Optical character of Er^{3+}/Yb^{3+} co-doped P_2O_5–CaO–Na_2O–Al_2O_3–AgO phosphate glass, Opt Commun. 284 (2011) 1868–1871, https://doi.org/10.1016/j.optcom.2010.12.011.
[63] H. Chen, Y.H. Liu, Y.F. Zhou, Z.H. Jiang, Spectroscopic properties of Er^{3+}-doped tellurite glass for 1.55 μm optical amplifier, J. Alloys Compd. 397 (2005) 286–290, https://doi.org/10.1016/j.jallcom.2004.12.051.
[64] Qiu-Hua Nie, Yuan Gao, Tie-Feng Xu, Xiang Shen, Investigation of thermal stability and spectroscopic properties in Er^{3+}/Yb^{3+}- codoped TeO_2–Li_2O–B_2O_3–GeO_2 glasses, Spectrochim. Acta, Part A 61 (2005) 1939, https://doi.org/10.1016/j.saa.2004.07.026, 1943.
[65] I. Jlassi, H. Elhouichet, M. Ferid, R. Chtourou, M. Oueslati, Study of photoluminescence quenching in Er^{3+}-doped tellurite glasses, Opt. Mater. 32 (2010) 743–747, https://doi.org/10.1016/j.optmat.2010.02.006.
[66] L. Li, Z. Zhou, H. Tian, D. Gong, Z. Yang, Y. Yang, Spectroscopic and upconversion properties of erbium-doped potassium lithium tantalate niobate crystals under 800 nm femtosecond laser excitation, J. Appl. Phys. 108 (2010) 043520, https://doi.org/10.1063/1.3475511.
[67] D.V.R. Murthy, A. Mohan Babu, B.C. Jamalaiah, L. Rama Moorthy, M. Jayasimhadri, Kiwan Jang, Ho Sueb Lee, Soung Soo Yi, Jung Hyun Jeong, Photoluminescence properties of Er^{3+} doped alkaline earth titanium phosphate glasses, J. Alloys Compd. 491 (2010) 349–353, https://doi.org/10.1016/j.jallcom.2009.10.179.